DOI 10.24425/aee.2025.154993

Design optimization of a non-uniform three-segment surface-inset Halbach permanent magnet synchronous motor

CAIXIA TAO^{®1}, ZEKUN LI^{®1™}, JIANGANG ZHANG^{®2}

¹School of Automation and Electrical Engineering, Lanzhou Jiaotong University Gansu Province China

²School of Mathematics and Science, Lanzhou Jiaotong University Gansu Province

e-mail: {1733425004/⊠ 523081009/35510377}@qq.com

(Received: 23.05.2025, revised: 25.08.2025)

Abstract: To solve the problem of excessive torque pulsation in surface-inset permanent magnet synchronous motors, a non-uniform three-segment surface-inset Halbach permanent magnet synchronous motor structure based on an eccentric magnetic pole is proposed. Firstly, the electromagnetic performance of the motor structure is analysed using the finite element method to establish the motor simulation model. Secondly, Pearson correlation analysis was used to stratify the initially motor structural parameters into strong and weak layers. Optimization is carried out using an improved multi-objective particle swarm optimization algorithm, Taguchi's method and parameter scanning method, respectively. Finally, simulation experiments were carried out using the finite element method and compared with the electromagnetic performance of the motor before optimization. The results show that the optimized proposed structure has suppressed the torque pulsations, significantly reduced the cogging torque, improved the air gap density sinusoidality and suppressed the harmonic amplitude, effectively improving the electromagnetic performance of the motor.

Key words: eccentric magnetic pole, Halbach array, layered optimization, permanent magnet synchronous machine

1. Introduction

Permanent magnet synchronous motors, as high output torque and high efficiency motors, are now widely used in aerospace, new energy vehicles, manufacturing and other fields [1–4]. According to the position of the magnetic poles on the rotor, permanent magnet motors are



© 2025. The Author(s). This is an open-access article distributed under the terms of the Creative Commons Attribution-NonCommercial-NoDerivatives License (CC BY-NC-ND 4.0, https://creativecommons.org/licenses/by-nc-nd/4.0/), which permits use, distribution, and reproduction in any medium, provided that the Article is properly cited, the use is non-commercial, and no modifications or adaptations are made. 738 Caixia Tao Arch. Elect. Eng.

divided into surface-type and embedded-type, where the surface-type rotor structure can be further divided into surface-mounted and surface-inset types. The surface-inset permanent magnet synchronous motor (SIPMSM) exhibits enhanced performance characteristics compared to surface-mounted permanent magnet synchronous motors. Specifically, the presence of salient poles in the SIPMSM introduces reluctance torque components, thereby improving both output torque and flux-weakening speed regulation capability. When compared to interior permanent magnet synchronous motors, the SIPMSM demonstrates superior manufacturing advantages as its permanent magnets are embedded into the rotor surface, requiring only slot machining on the rotor exterior. This configuration significantly reduces production costs and simplifies maintenance procedures. The current optimization and improvement of the SIPMSM mainly focuses on the improvement of the magnet structure. These modifications aim to optimize electromagnetic performance while maintaining structural simplicity [5–7].

In terms of motor topology design, the permanent magnet pole-shaving technique can effectively improve the sinusoidality of the air-gap magnet density of permanent magnet synchronous motors. Currently, the eccentric and sinusoidal cutting methods are more commonly used [8]. Eccentric pole cutting is a cutting method in which the upper surface of the pole is designed as an eccentric arc, and the shape of the pole can be changed by changing the eccentricity of the arc, the thickness of the permanent magnet, and the pole arc coefficient [9, 10]. Reference [11] introduced eccentric pole cutting into the SIPMSM, used the Taguchi method to assist the agent model modelling, and then used the genetic algorithm to optimize the motor model, the optimized model reduces the cogging torque and torque pulsation compared to the initial SIPMSM model, and improves the average torque of the motor, but the optimization has some limitations because of fewer parameters considered. Changing the magnetization direction of the magnetic poles, such as using Halbach arrays, by changing the magnetization direction of the permanent magnets, the magnetic circuit of the magnetic poles can be changed so that a strong magnetic field is generated on one side, which improves the no-load air-gap magnetic density waveform of the motor and reduces the cogging torque and torque pulsation. The more the number of blocks per pole of the Halbach array permanent magnet, the better the magnetic field distribution optimization effect, but with the increase in the number of blocks, the manufacturing process difficulty and cost will increase. Considering the optimization effect and the realization difficulty, 3 blocks per pole is the most suitable, i.e., the three-segment Halbach array permanent magnet structure [12]. Reference [13] proposes an improved Halbach permanent magnet synchronous motor structure to reduce the motor cogging torque and torque pulsation by changing the built-in magnetic pole magnetizing method, but the difficulty of manufacturing the rotor structure is not considered.

Optimization of motor parameters using multi-objective optimization algorithms is an approach that combines motor optimization with the computer field to efficiently improve motor performance and reduce motor production costs. For the improvement of the optimization method, References [14, 15] improve the inertia weight updating formula in the multi-objective particle swarm optimization (MOPSO) algorithm, and enhance the global search capability at the initial stage of the algorithm and the local search capability at the later stage of the algorithm, in order to improve the search capability of MOPSO. It is proved that the improvement of inertia weights can improve the efficiency of motor optimization. Reference [16] proposes a hierarchical iterative optimization strategy based on NSGA-II, which solves the problem of the traditional hierarchical optimization method of ignoring the weak layer parameter which makes it difficult to ensure whether the final

parameter is optimal or not, but the optimization search of the NSGA-II algorithm used is more complicated. Taguchi's method, as an experimental design method, has also been applied by many scholars to the multi-objective optimization problem of electric machines [17]. Existing improvements to Taguchi's method mainly use an iterative approach. References [18, 19] apply the improved iterative Taguchi's method to the multi-objective optimization problem of electric machines, which improves the optimization accuracy compared to traditional Taguchi's method, but at the same time the introduction of iteration greatly increases the computation time. As proposed by [20], an optimization method was developed which utilizes a multi-layer agent model. It was hypothesized that the parameters resulting from multi-dimensionality reduction would facilitate multi-objective search processes, and that the effectiveness of the multi-layer optimization method would be substantiated by a comparative analysis with the traditional multi-field coupling optimization method for electric machines.

In this paper, an eccentric non-uniform Halbach SIPMSM structure (ENHSIPMSM) is proposed to address the problem of excessive torque pulsation in table-plugged permanent magnet synchronous motors. This structure consists of two auxiliary poles with the main pole being an eccentric pole cutting. Firstly, a comparative analysis of the electromagnetic performance of the ENHSIPMSM using the finite element method reveals that certain properties of the ENHSIPMSM outperform those of the other SIPMSM structures. It is evident that there is potential to improve the ENHSIPMSM's electromagnetic performance. Secondly, correlation analysis was conducted on the selected optimization parameters of the ENHSIPMSM. The correlation analysis results were then used to divide the selected optimization parameters into three layers: strong, medium and weak. The optimization process is achieved through the implementation of a Response Surface Model (RSM) agent model in conjunction with an improved MOPSO algorithm, the Taguchi method and a parameter scanning method, respectively. Finally, the performance of the motor before and after optimization is compared by finite element simulation to verify the superiority of the proposed motor and the optimization method.

2. Motor topologies

In this paper, the focus is on a propulsion motor with a rated power of 10 kW. The fundamental parameters of the motor are delineated in Table 1.

Parameter	Value	Parameter	Value
Rated power/kW	10	Stator outer diameter/mm	215
Rated speed/(r/min)	600	Stator inner diameter/mm	118
Pole pairs	4	Rotor outer diameter/mm	104

Table 1. Motor basic parameter

Continued on next page

Table 1 – Continued from previous page

Parameter Va		Parameter	Value
Supply frequency/Hz	40	Pole thickness/mm	5
Stator slots	48	Rotor yoke thickness/mm	5
Pole arc ratio	0.9	Stator slot depth/mm	33
Core length/mm	250	Stator slot opening width/mm	3.5

In order to reduce the torque pulsation and cogging torque of the SIPMSM structure, the ENHSIPMSM rotor structure is proposed in this paper. The comparison of the SIPMSM, non-uniform Halbach SIPMSM (NHSIPMSM) and ENHSIPMSM is shown schematically in Fig. 1.

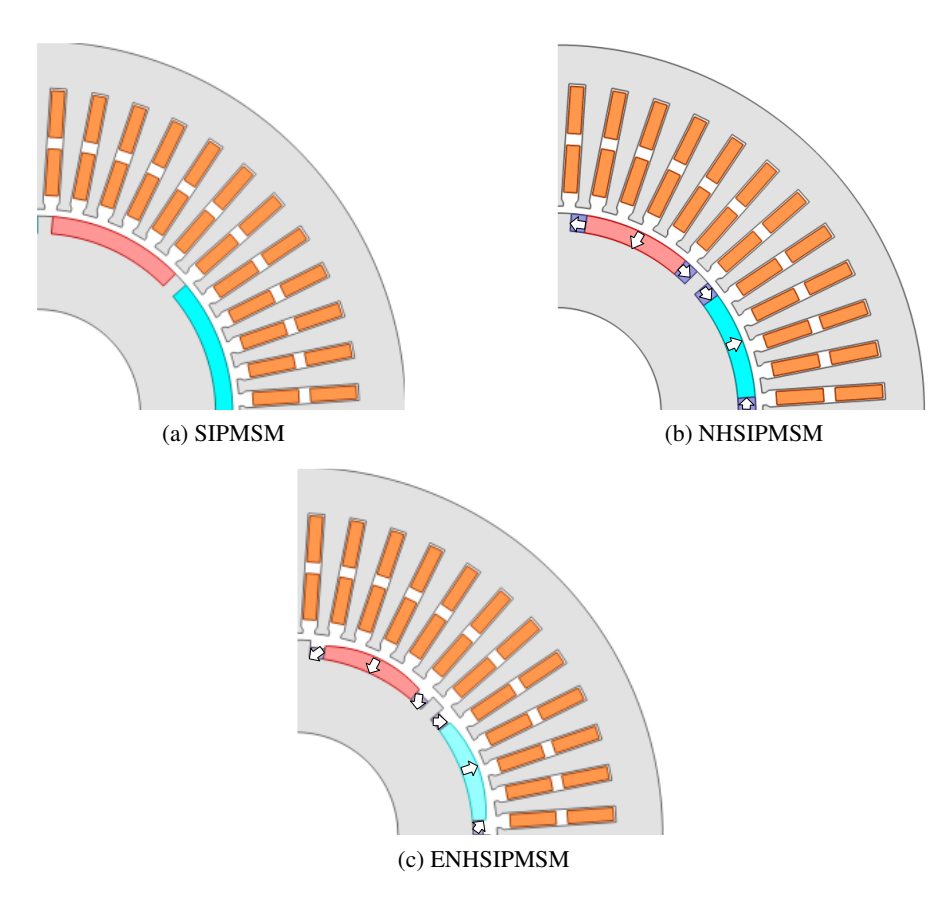


Fig. 1. Schematic of three motor configurations

The eccentric pole cutting method involves the utilization of an eccentric arc as the upper surface of the pole. The objective of this approach is to enhance the waveform of the air gap magnetization by modifying the shape of the pole. Figure 2 presents a schematic representation of the ENHSIPMSM permanent magnet.

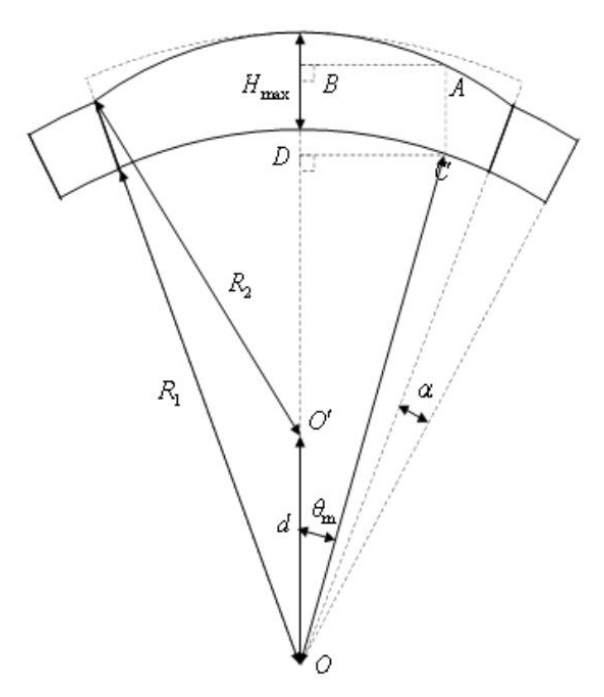


Fig. 2. Schematic of ENHSIPMSM magnetic pole configuration

There, O is the center of the arc circle on the upper surface of the magnetic pole in front of the cutting pole, O' is the center of the arc on the upper surface of the pole after cutting and d is the eccentricity of the eccentric arc. It is possible to alter the configuration of the upper surface of the pole by modifying the eccentricity distance d and the main pole arc coefficient n_1 . H_{max} is the maximum thickness of the permanent magnet. n_2 is the pole-arc coefficient of a single auxiliary pole.

According to the established geometrical relationship, the thickness of the primary pole, measured in units of length, is directly proportional to the angle θ_m , measured in units of angular measure, between the pole midline and the OC. This relationship is expressed as follows:

$$h(\theta_m) = d + \sqrt{(H_{\text{max}} + R_1 - d)^2 - (R_1 \sin \theta_m)^2} - R_1 \cos \theta_m.$$
 (1)

The same fundamental parameters are employed for the three motor configurations, with the ENHSIPMSM initial model parameters displayed in Table 2.

Table 2. ENHSIPMSM initial model parameters

Parameters	Value
Eccentricity distance d/mm	20
Maximum thickness of permanent magnet H_{max}/mm	5
Thickness of auxiliary magnetic pole H_f /mm	3
Pole arc coefficient of main magnetic pole n_1	0.7
Pole arc coefficient of single auxiliary magnetic pole n_2	0.1
Magnetization angle of auxiliary magnetic pole/deg	45
Outer diameter of stator D_y /mm	215
Inner diameter of stator D_g /mm	118
Slot opening width of stator B_{s0} /mm	3.5

3. Electromagnetic characteristics

3.1. Analysis of the magnetic field

Through the finite element simulation experiments under no-load conditions of the motor, the motor magnetization cloud diagrams of the three motor structures are obtained, as shown in Fig. 3.

The maximum magnetic densities of the SIPMSM, NHSIPMSM, and ENHSIPMSM in Fig. 3 are 2.6510 T, 1.9769 T, and 2.3116 T, respectively. It can be seen that the ENHSIPMSM achieves a larger magnetization capacity with fewer permanent magnets when the permanent magnets are also NdFeB.

Ideally, the radial air gap density distribution in the motor should be sinusoidal, which produces a smooth electromagnetic torque and reduces torque pulsation, Fast Fourier Transform (FFT) of the radial air gap density of a motor separates the fundamental and harmonic components to help evaluate the performance of the motor. Figure 4 shows the comparative analysis of the radial air gap magnetic density.

From Fig. 4(a), it can be seen that the radial air gap magnetization amplitude sinusoidality of the ENHSIPMSM structure is better compared to other motors, which is conducive to the output of stable electromagnetic torque. From the results of the Fourier analysis of the radial magnetic density in Fig. 4(b), the lower amplitude of the fundamental wave of the ENHSIPMSM structure is obtained, which is mainly due to the reduction of the magnetic pole usage. The 3rd, 5th, and 7th harmonic amplitudes are reduced to varying degrees, and these lower harmonics are the primary source of torque pulsations. Furthermore, higher harmonics are also marginally diminished. The total harmonic distortion (THD) of radial airgap magnetic flux density of the ENHSIPMSM is 14.07%, which is the smallest value when compared to other structures. The findings demonstrate that the optimized motor structure design effectively suppresses harmonics, thereby ensuring enhanced motor stability.

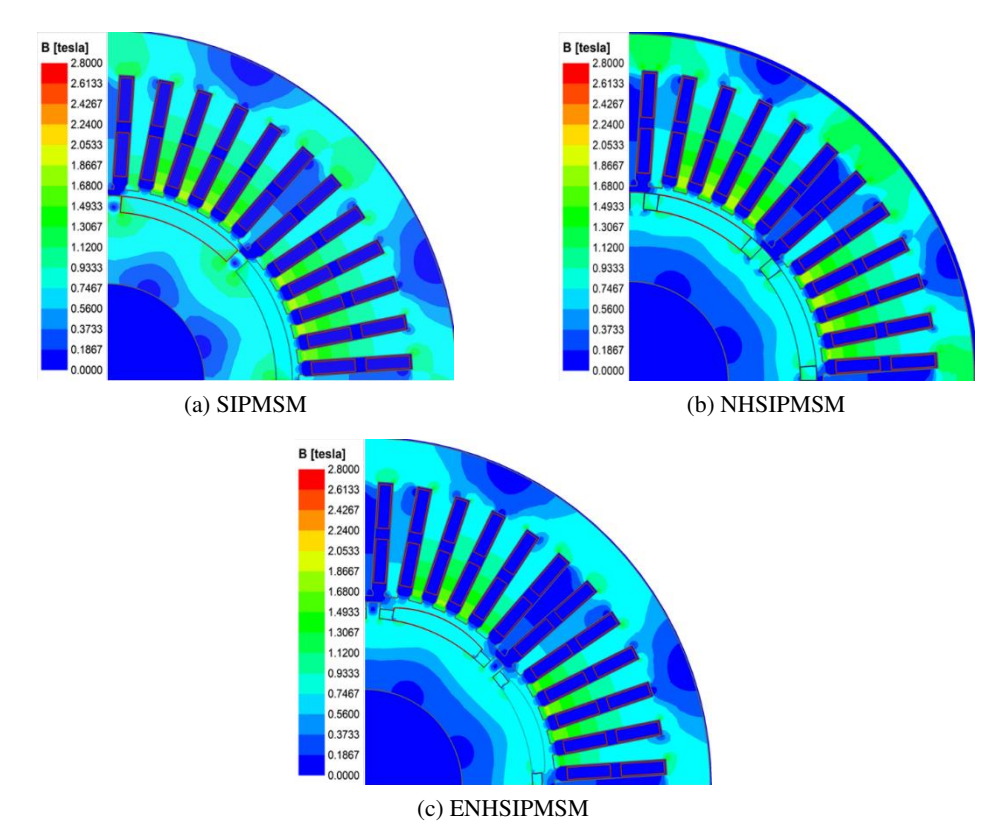


Fig. 3. Magnetic flux density contour plot of the motor

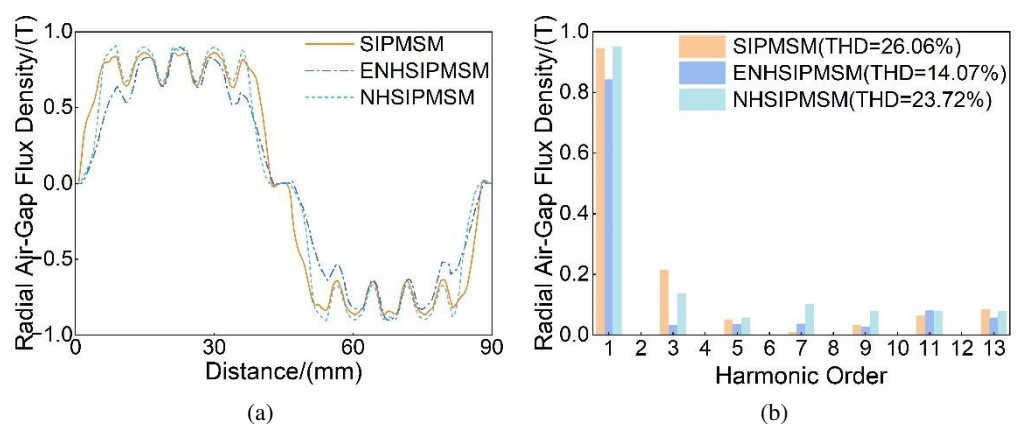


Fig. 4. Comparison of airgap flux densities: radial airgap flux density waveform (a); FFT spectra comparison of radial airgap flux density (b)

744 Caixia Tao Arch. Elect. Eng.

3.2. Analysis of electromagnetic torque

Torque pulsation has been shown to have a detrimental effect on the operation of the motor. Excessive torque pulsation can result in fluctuations in motor speed and vibrations, which, in turn, generate noise. The calculation of the average motor output torque T_{avg} and torque pulsation T_r is achieved through the utilization of the following formula:

$$T_{\text{avg}} = \frac{1}{T} \int_{0}^{T} T_{e}(t) dt, \qquad (2)$$

$$T_r = \frac{T_{e \text{ max}} - T_{e \text{ min}}}{T_{e \text{ min}} + T_{e \text{ min}}} \times 100\%,$$
 (3)

where T_e is the electromagnetic torque; $T_{e \text{ min}}$ is the minimum value of electromagnetic torque; and $T_{e \text{ max}}$ is the maximum value of electromagnetic torque.

Finite element simulation experiments were performed at rated operating conditions, and the electromagnetic torque of the three motor configurations is shown in Fig. 5.

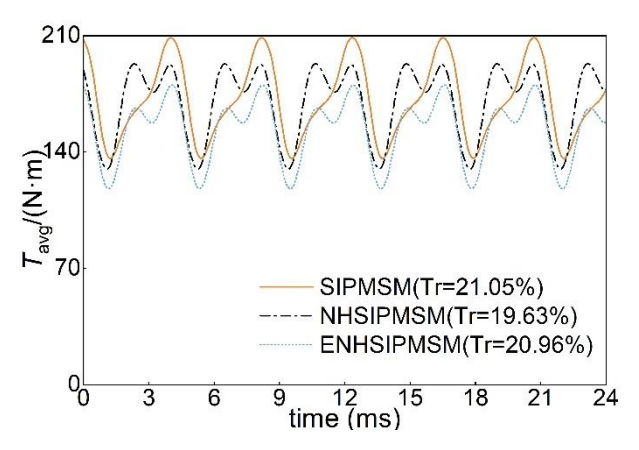


Fig. 5. Analysis of electromagnetic torque characteristics

As demonstrated in Fig. 5, the ENHSIPMSM configuration exhibits a comparatively diminished electromagnetic torque in comparison to the other models, primarily attributable to a decrease in the quantity of permanent magnets. Furthermore, the torque pulsations observed in the ENHSIPMSM structure are reduced relative to the initial SIPMSM model.

3.3. Analysis of cogging torque

Cogging torque is the result of the tangential component of the interaction force between the permanent magnets and the armature teeth. The combined effect of cogging torque and reluctance torque is responsible for torque pulsations and noise during SIPMSM operation. The motor

cogging torque T_{cog} , calculated using the Maxwell tensor method, is expressed as follows:

$$T_{\text{cog}} = \frac{L_a R_{av}^2}{\mu_0} \int_0^{2\pi} B_r B_t d\theta, \tag{4}$$

where L_a is the length of the motor core; R_{av} is the radius at the center position of the air gap; μ_0 is the vacuum permeability; B_r is the radial component of the air gap magnetic density; and B_t is the directional component of the air gap magnetic density.

Finite element simulation experiments were conducted under no-load conditions, and the cogging torque of the three motor structures is shown in Fig. 6.

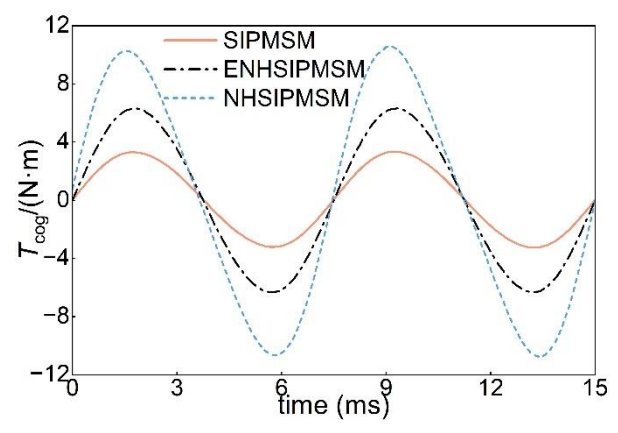


Fig. 6. Analysis of cogging torque

The initial ENHSIPMSM structure demonstrates a high cogging torque, necessitating subsequent optimization of the structural parameters through the implementation of a multi-objective optimization method.

4. Layered optimized design

4.1. Layered optimization process

In layered optimization methods, the parameters are generally stratified according to the relevance of their effect on the objective function, and then they are optimized separately. The purpose of using a layered optimization approach is to reduce the dimensionality of the multi-objective optimization problem and make the optimization process more controllable and easier to converge. However, it should be noted that layered optimization methods can only output a single solution.

In this paper, by dividing the parameters into three layers, the multi-objective optimization problem can be further reduced to a lower dimension. The optimization process is simplified by using different optimization methods for different correlation parameters. A multi-objective motor optimization flowchart is shown in Fig. 7.

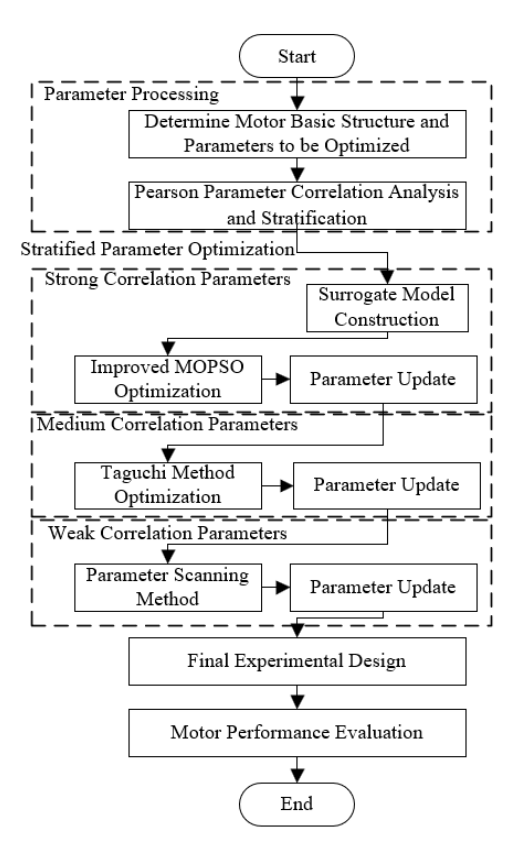


Fig. 7. Multi-objective motor optimization flowchart

4.2. Parameter pre-processing

The maximum average output torque $T_{\rm avg}$, the minimum torque pulsation T_r , and the minimum cogging torque peak $T_{\rm cog}$ obtained in this paper are taken as the optimization targets to further improve the motor performance and increase the stability and lifetime of the motor operation. The optimization parameters associated with the optimization objective are selected, and a reasonable optimization range is designated. The range of parameters to be optimized is delineated in Table 3.

Parameter	Value	Parameter	Value
d/mm	5~35	D_g /mm	116~120
n_1	0.6~0.7	D _y /mm	200~230
H_f /mm	0~5	B _{s0} /mm	2~5
H _{max} /mm	4.5~5.5	θ/deg	0~90
n_2	0.05~0.15		

Table 3. Optimization parameters ranges

4.3. Parameter correlation analysis

Correlation analysis measures the proximity of variables and factors. It identifies which variables to optimize that significantly impact the motor's performance, so the motor design can be targeted for optimization. In this paper, Pearson correlation analysis is employed to establish different levels of parameter strength. The Pearson coefficient can be expressed as follows:

$$\rho_{XY} = \frac{\sum_{i=1}^{n} \left(X_i - \overline{X} \right) \left(Y_i - \overline{Y} \right)}{\sqrt{\sum_{i=1}^{n} \left(X_i - \overline{X} \right)^2} \sqrt{\sum_{i=1}^{n} \left(Y_i - \overline{Y} \right)^2}},$$
(5)

where *X* is the parameter variable, *Y* is the optimization objective, and *n* is the number of samples. The value domain of the parameter ρ ranges from -1 to 1. The magnitude of the absolute value of ρ_{XY} is directly proportional to the strength of the correlation between the parameters.

Each design variable exhibits a different degree of correlation with the optimization objective. Therefore, it is difficult to select the key design variables solely based on the results of the corresponding correlation coefficients. To address this issue, this paper employs the trade-off correlation coefficient analysis. The composite correlation coefficient of the selected design variables is as follows:

$$S_{\text{com}}(X) = \sum_{i=1}^{n} \omega_i \cdot \rho_{XY_j}, \tag{6}$$

where ω_i is the weight of the parameter associated with each optimization objective. The problem of excessive torque pulsation in the ENHSIPMSM is addressed in the paper through the following methodology: the magnitude of the weights associated with the three objective functions is established as 0.25, -0.25 and -0.5, respectively. The ensuing results of the Pearson correlation analysis are displayed in Fig. 8.

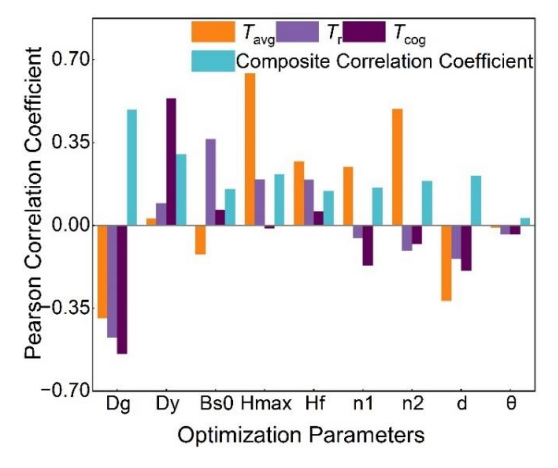


Fig. 8. Pearson correlation analysis results

748 Caixia Tao Arch. Elect. Eng.

Based on a comprehensive analysis of Pearson correlation results, the parameters were classified into three categories as follows: strong-layer parameters were defined as those with a comprehensive correlation coefficient greater than 0.2 and absolute correlation values with two or more objective functions exceeding 0.1. These included D_g , H_{max} , and d; medium-layer parameters were identified as those with a comprehensive correlation coefficient between 0.1 and 0.2 and absolute correlation values with two or more objective functions exceeding 0.1, such as B_{s0} , H_f , and n_1 ; weak-layer parameters comprised those with either a comprehensive correlation coefficient less than 0.1 or absolute correlation values with two or more objective functions below 0.1, including D_y , n_2 , and θ .

4.4. Strong-layer parameters optimization

The influence of the strong-layer parameters on the objective function is very significant. There is usually a complex nonlinear coupling between the optimization parameters. The computational cost of solving strong layer parameter optimization problems using only the finite element method is too high. It takes close to 30 min to perform a single finite element analysis. The utilization of the RSM facilitates a surrogate model from a modest amount of simulation experimental data, thereby capturing nonlinearities and the interactive effects between parameters and responses. This approach provides precise predictions concerning global optimization.

MOPSO introduces elite pooling and mutation operations to particle swarm optimization, has strong multi-objective optimization capabilities, and is simple and easy to operate compared to other algorithms. Therefore, in this paper, we choose to improve MOPSO to complete the optimization search. It should be ensured that the particles prioritize global search during the pre-optimization phase and local search during the post-optimization phase, thereby averting the tendency to settle on local optimal solutions. The present study employs enhanced nonlinear decreasing inertia weights [15] and velocity pause [21]. The velocity update equations of the improved MOPSO algorithm are given by Eqs. (7) and (8).

$$\omega = \lambda_1 \exp\left(\frac{1}{1 + \lambda_2 k/T}\right),\tag{7}$$

$$\omega = \lambda_1 \exp\left(\frac{1}{1 + \lambda_2 k/T}\right), \tag{7}$$

$$v_i(t+1) = \begin{cases} v_i(t) & \text{if rand } > \alpha \\ \omega v_i(t) + c_1 r_1(p \text{best}_i(t) - x_i(t)) + c_2 r_2(g \text{best}(t) - x_i(t)) & \text{Otherwise} \end{cases}, \tag{8}$$

where T is the maximum number of iterations; t is the current number of iterations; λ_1 and λ_2 are the control parameters, which are taken as 0.33 and 4, respectively, so that ω decreases from 0.9 to 0.4 nonlinearly.

To verify the effectiveness of the improved MOPSO, it is compared to the MOPSO algorithm with nonlinear inertia weight (NIW) and fixed inertia weight (FIW). In this paper, the DTLZ3 test function is selected, the population size is 300, the number of iterations is 500, and each algorithm is run 10 times. The evaluation of the algorithm's performance is done in terms of generation distance (GD) and spacing (SP). A smaller value of GD indicates a higher convergence of the algorithm, and a smaller value of SP means that the algorithm solution set is more evenly distributed in space. The results of the algorithm's test are presented in Table 4. As can be seen from Table 4, the GD and SP values of the optimized MOPSO algorithm are smaller than the other two algorithms, which proves that the optimized MOPSO algorithm has more superior performance.

	Improved MOPSO	MOPSO-NIW	MOPSO-FIW
Average GD	0.52	0.56	0.88
GD Std. Dev.	0.271	0.277	0.34
Average SP	1.63	1.84	1.97
GD Std. Dev.	1.14	1.41	1.38

Table 4. Algorithm test results

An RSM develops an approximate mathematical model between the input factors and the output response through a design of experiments, highly accurate models can be obtained using low experimental costs. Using the Box-Behnken design (BBD) sampling method, an RSM was obtained using only 12 experiments. We employ second and third order polynomial response surface models, such as (9):

$$\begin{cases} y = a_0 + \sum_{i=1}^n b_i x_i + \sum_{i=1}^n \sum_{j=1}^n c_{ij} x_i x_j \\ y = a_0 + \sum_{i=1}^n b_i x_i + \sum_{i=1}^n \sum_{j=1}^n c_{ij} x_i x_j + \sum_{i=1}^n \sum_{j=1}^n \sum_{k=1}^n d_{ijk} x_i x_j x_k \end{cases}$$
(9)

The RSM is established through a meticulous analysis of the resultant data. The multi-objective optimization function is obtained as shown in (10):

$$T_{\text{avg}} = -10580 + 183.48D_g + 31.43H_{\text{max}} - 5.00d + 0.037D_g d + 0.068H_{\text{max}} d$$

$$-0.80D_g^2 - 0.013d^2,$$

$$T_{\text{cog}} = -59287 + 996.25D_g + 12658.43H_{\text{max}} - 3.83d - 212.63D_g H_{\text{max}} + 0.043D_g d$$

$$-0.27H_{\text{max}} d - 4.183D_g^2 + 2.615H_{\text{max}}^2 + 0.892D_g^2 H_{\text{max}},$$

$$T_r = 13483 - 222.28D_g - 30.152H_{\text{max}} + 0.555d - 0.143H_{\text{max}} d$$

$$+0.922D_g^2 + 3.078H_{\text{max}}^2.$$
(10)

The RSM fit was measured using the coefficient of the determination R^2 . The RSM objective functions exhibit R^2 values of 0.999, 0.991, and 0.991, respectively. This finding indicates that the RSM fit is more effective.

We aimed to achieve optimized results featuring increased average torque, reduced torque ripple and cogging torque. The filtered solutions are then subjected to a process of normalization, after which the weighted value is employed as the score for the group of solutions. The highest rated solution among them is taken as the optimal solution, and the normalized and weighted formulas are shown in (11) and (12):

$$x' = \frac{x - X_{\min}}{X_{\max} - X_{\min}},$$

$$S = \omega_1 \times T'_{\text{avg}} + \omega_2 \times T'_{\text{cog}} + \omega_3 \times T'_r,$$
(11)

$$S = \omega_1 \times T'_{\text{avg}} + \omega_2 \times T'_{\text{cog}} + \omega_3 \times T'_r, \tag{12}$$

where x is the parameter to be normalized, S is the score of the solution, and T'_{avg} , T'_{cog} and T'_r are the normalized values. The three weights are 0.25, -0.25, and -0.5, respectively, the symbols before the weights represent the direction of optimization.

The optimization of the objective function using the improved MOPSO results in the Pareto front plot is depicted in Fig. 9. The optimization results of the strong-layer parameters are presented in Table 5. As a supplementary note, the optimal individuals marked in Fig. 9. are obtained from algorithmic optimization, and Table 5 is obtained from the finite element method. Since the optimization objective of the algorithm is a predictive model, there is some deviation from the actual model, but the error results are within acceptable limits.

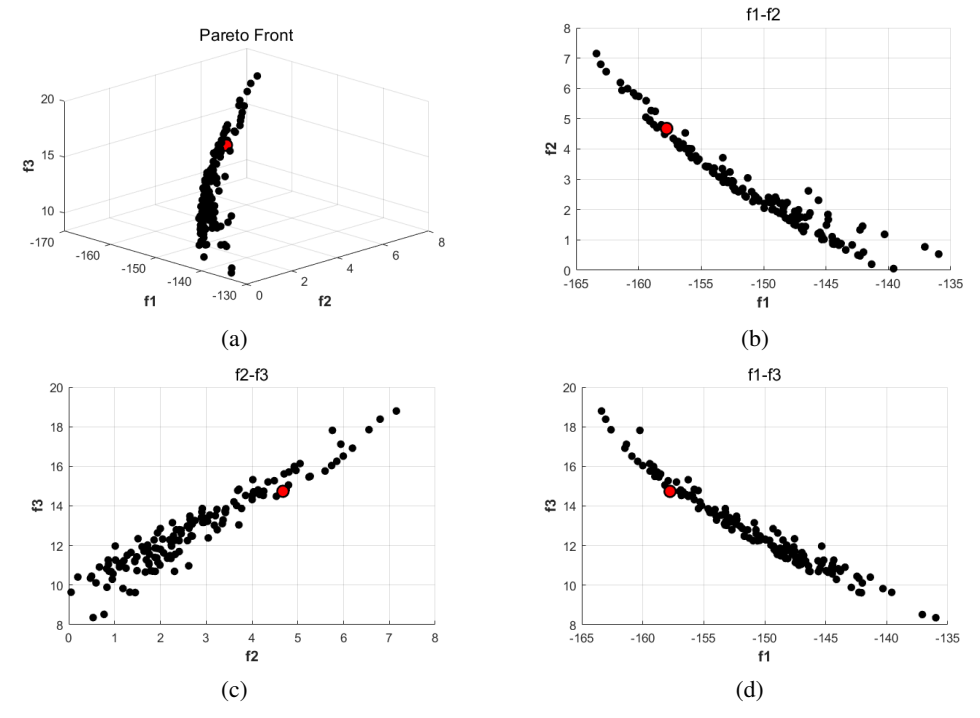


Fig. 9. Pareto front plot: 3D pareto front (a); f1–f2 plane projection (b); f2–f3 plane projection (c); f1–f3 plane projection (d)

Table 5. Strong-layer parameters optimization results

	Pre optimization	After optimization
d/mm	20	24.98
D_g /mm	118	118.97
h _{max} /mm	5	5.49
$T_{\text{avg}}/(\mathbf{N}\cdot\mathbf{m})$	154.30	157.26
$T_{\text{cog}}/(\mathbf{N}\cdot\mathbf{m})$	6.32	5.02
T_r /%	20.96	14.02

4.5. Medium-layer parameters optimization

The medium-layer parameters demonstrate a moderate correlation with the objective function, and the design space is relatively straightforward. In the present paper, we have opted to utilize Taguchi's methodology for the optimization of the medium-layer parameters. Taguchi's method aims to find the optimal combination of parameters in the system by minimizing the number of experiments to quickly find the optimal level by signal-to-noise ratio analysis.

The selection of three levels was made on the basis of the range of values exhibited by the parameters in question, the establishment of the orthogonal tables $L_9(3^3)$ followed this initial selection. The necessity of only 9 simulation experiments is a substantial reduction in the number of experiments when compared to the 3³ simulation experiments required by the traditional test method permutation. The level values selected for the Taguchi method are enumerated in Table 6.

Optimization parameters	B_{s0} /mm	H_f /mm	n_1
Level 1	2	1	0.6
Level 2	3.5	3	0.65
Level 3	5	5	0.7

Table 6. Number of parameter levels optimized via Taguchi method

The orthogonal test table was designed according to the optimized parameter levels selected in Table 6, and electromagnetic simulation was performed using the finite element method for the combination of nine experiments in the orthogonal experimental table. A comparison of signal-to-noise ratios is conducted through the utilization of calculation types "look big" and "look small". Mathematical expressions are as in Eqs. (13) and (14):

$$S/N = -10\log_{10}\left(\frac{1}{k}\sum_{i=1}^{k}\frac{1}{X_i^2}\right),$$

$$S/N = -10\log_{10}\left(\frac{1}{k}\sum_{i=1}^{k}X_i^2\right).$$
(13)

$$S/N = -10\log_{10}\left(\frac{1}{k}\sum_{i=1}^{k}X_i^2\right). \tag{14}$$

Assign 0.25, 0.25, and 0.5 to the objective function T_{avg} , T_{cog} , and T_r signal-to-noise (S/N) weights, respectively, and calculate the integrated signal-to-noise ratio.

The results of orthogonal tests are shown in Table 7. The values of B_{s0} , H_f and n_1 in the level of the maximum value of the integrated signal-to-noise ratio are 2 mm, 3 mm, and 0.65, respectively.

Table 7. Orthogonal array $L_9(3^3)$ experimental results

Number of trials	<i>B</i> _{s0} /mm	H_f /mm	n_1	$T_{\rm avg}/({ m N\cdot m})$	$T_{\text{cog}}/(\mathbf{N}\cdot\mathbf{m})$	T _r /(%)	Integrated S/N
1	2	1	0.6	132.16	2.07	20.44	15.92

Continued on next page

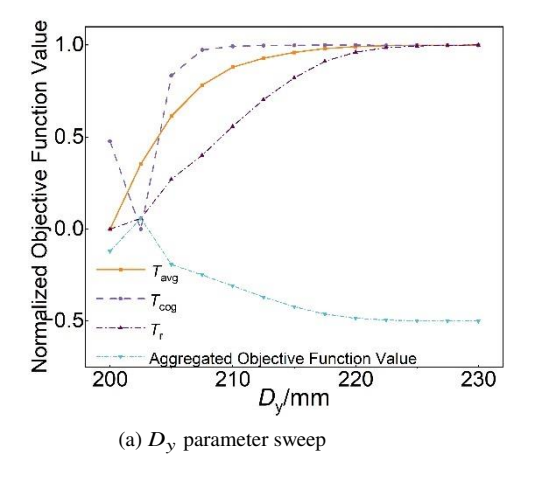
752 Caixia Tao Arch. Elect. Eng.

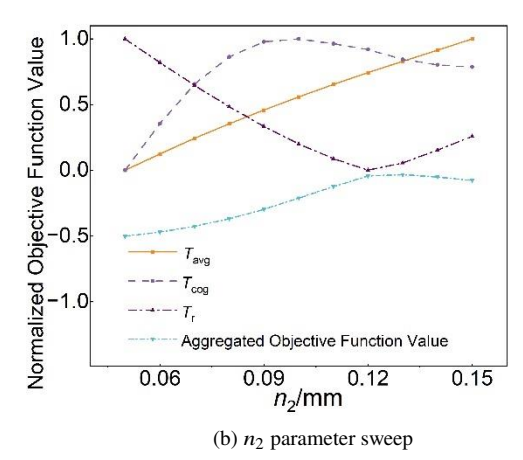
Table 7 – *Continued from previous page*

Number of trials	<i>B</i> _{s0} /mm	H_f /mm	n_1	$T_{\text{avg}}/(\mathbf{N}\cdot\mathbf{m})$	$T_{\text{cog}}/(\mathbf{N}\cdot\mathbf{m})$	T _r /(%)	Integrated S/N
2	2	3	0.65	150.95	1.29	14.27	18.79
3	2	5	0.7	168.07	4.02	18.72	15.38
4	3.5	1	0.6	131.34	5.72	23.05	13.18
5	3.5	3	0.7	157.26	5.02	14.02	15.64
6	3.5	5	0.65	162.26	14.42	23.82	11.49
7	5	1	0.7	146.17	5.63	15.50	15.17
8	5	3	0.65	146.05	5.01	13.92	15.89
9	5	5	0.6	149.73	2.25	17.13	16.78

4.6. Weak-layer parameters optimization

Weak-layer parameters are those that have weak effects on most targets or show significant correlation only in a few targets. The parameter scanning method is employed to optimize in accordance with the strength of the integrated correlation D_y , n_2 , and θ , contingent upon the determination of the preceding optimization results and the results of the three objective parameters are normalized. The three objective functions (T_{avg} , T_r , and T_{cog}) are assigned weights of 0.25, -0.25, and -0.5, respectively, to construct a composite function that is used to determine the performance advantages and disadvantages. The optimal values of D_y , n_2 , and θ are obtained as 202.5 mm, 0.13, and 40 deg, respectively, according to the parametric scanning process in Fig. 10.





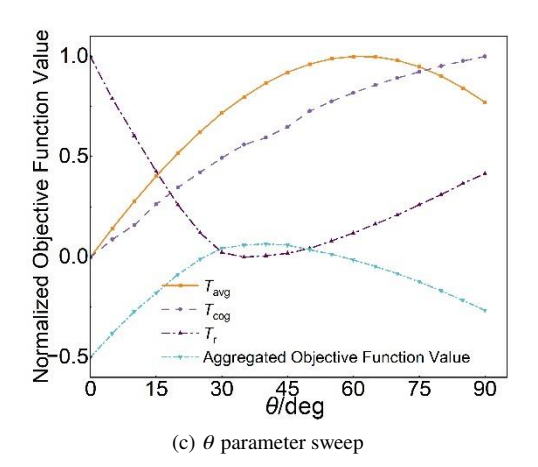


Fig. 10. Parameter sweep results

5. Optimization results analysis

In order to verify the validity of the parameters after improved hierarchical optimization, the optimized ENHSIPMSM structure was analyzed in comparison with the pre-optimization ENHSIPMSM using the finite element method. The comparative analysis of electromagnetic torque is illustrated in Fig. 11. The optimized ENHSIPMSM structure demonstrates minimal reduction in electromagnetic torque; however, torque pulsation is reduced by 84.07% in comparison to the pre-optimization period. The optimized ENHSIPMSM output torque demonstrates enhanced stability.

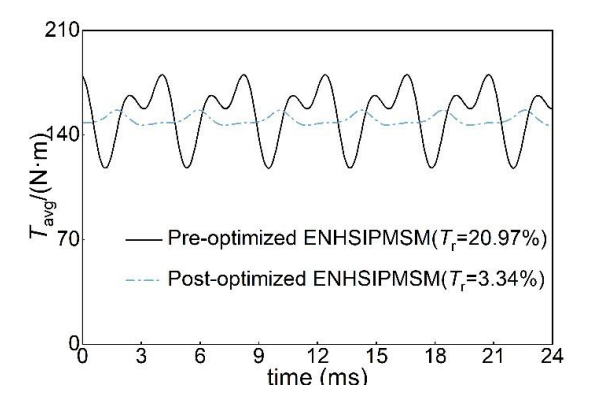


Fig. 11. Comparison of electromagnetic torque before and after optimization

As demonstrated in Fig. 12, the analysis indicates 81.51% reduction in the cogging torque of the optimized ENHSIPMSM structure in comparison to the pre-optimization ENHSIPMSM structure. This will effectively reduce vibration and noise during motor operation, thereby improving the overall operating efficiency of the motor and prolonging its service life.

Comparative analysis of radial air gap magnetism in Fig. 13 shows that the sinusoidal degree of the optimized ENHSIPMSM radial air gap magnetism is more excellent compared to the

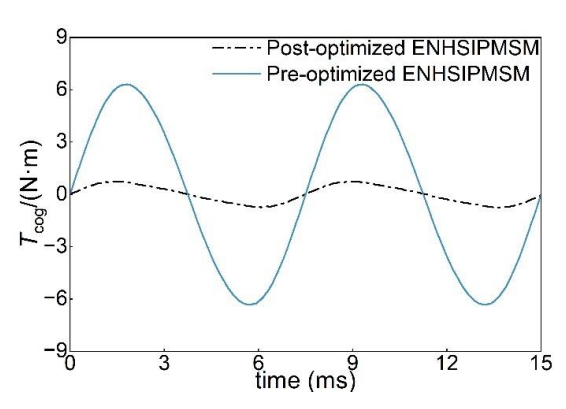


Fig. 12. Comparison of cogging torque before and after optimization

pre-optimization period, and THD of the radial air gap magnetism decreases from 14.07% to 8.12% compared to the pre-optimization period, which is a decrease of 42.29%. From Fig. 13(b), it can be obtained that the base wave amplitude of the radial air-gap magnetic density of the optimized ENHSIPMSM is improved as compared to the pre-optimization, and almost all the harmonic amplitudes are reduced as compared to the pre-optimization, and the stability of the operation of the motor structure will be improved.

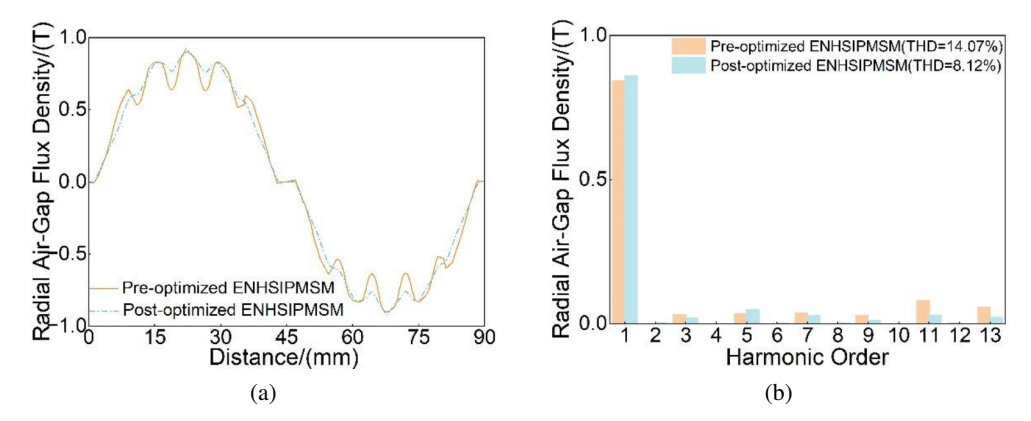


Fig. 13. Comparison of radial airgap flux density before and after optimization: radial airgap flux density waveform (a); FFT spectra comparison of radial airgap flux density (b)

6. Conclusions

- 1. In order to solve the problem of excessive torque pulsation in SIPMSMs, this paper proposes a non-uniform Halbach array SIPMSM structure composed of two auxiliary poles with the main pole being an eccentric cutting pole.
- 2. The ENHSIPMSM structure, as delineated in this paper, exhibits enhanced electromagnetic performance following hierarchical optimization. The optimized ENHSIPMSM demonstrates minimal reduction in electromagnetic torque when compared to the pre-optimized

- ENHSIPMSM structure. However, a substantial decrease of 84.07% in torque pulsation is observed when contrasted with the pre-optimized configuration, 81.51% reduction in cogging torque. The radial air-gap density waveform sinusoidal degree demonstrates superior performance, achieving a 42.29% reduction in radial air-gap density THD.
- 3. The optimized ENHSIPMSM significantly improves the stability of the motor during operation while reducing the number of permanent magnets compared to the SIPMSM. The employment of improved MOPSO and multilayer hierarchical optimization methods offers an alternative approach to addressing multi-objective optimization problems for electric machines.

Acknowledgements

The paper was supported by the National Natural Science Foundation of China (62463016), the Gansu Province Science and Technology Program Grant (No.23JRRA880), the Key Project of the Gansu Natural Science Foundation (No.23JRRA882), and the Industrial Support and Guidance Project of Colleges and Universities of Gansu Province (No.2024CYZC-23).

References

- [1] Li Shubin, Zhou Lawu, Wang Xiaofei, Dai Zhenhui, *Parameter optimization design of double-layer magnets permanent magnet synchronous motor for vehicles based on multi-round evolutionary algorithm*, Science Technology and Engineering (in Chinese), vol. 24, no. 23, pp. 9891–9898 (2024), DOI: 10.12404/j.issn.1671-1815.2306748.
- [2] Wei Jialin, Wang Youlong, Wen Xuhui, Chen Chen, Li Wenshan, *Analysis and design of 300 kW aerospace high-speed PM generator*, Electric Machines and Control (in Chinese), vol. 27, no. 9, pp. 63–72 (2023), DOI: 10.15938/j.emc.2023.09.007.
- [3] Zhang Lei, Bao Jiusheng, Ge Shirong, Yang Xiaolin, Yin Yan, Bao Jiuyang, *Permanent magnet driving technology and its application status in the field of mining equipment*, Coal Science and Technology (in Chinese), vol. 50, no. 3, pp. 275–285 (2022), DOI: 10.13199/j.cnki.cst.2020-0226.
- [4] Caixia Tao, Yaogeng Zhang, Fengyang Gao, Jiangang Zhang, *Study on the weakening of stator cogging torque of modular motors by gap offsets*, Archives of Electrical Engineering, vol. 73, no. 3, pp. 779–798 (2024), DOI: 10.24425/aee.2024.150895.
- [5] Bao Xiaohua, Wu Changjiang, Hu Tunpeng, Wang Chunyu, A method for optimizing performance of inset permanent magnet motor, Transactions of China Electrotechnical Society (in Chinese), vol. 33, no. 2, pp. 238–244 (2018), DOI: 10.19595/j.cnki.1000-6753.tces.170358.
- [6] Du Xinxin, Research on the method of reducing torque ripple for surface-insert permanent magnet motor based on magnet shifting, Master's Thesis, Jiangsu University, Zhenjiang (2018).
- [7] Li Dalin, Hua Hao, Li Ran, Xu Shaolun, Qi Wenjuan, *Torque improvement for high power density machines with shifted surface-inserted permanent magnets*, Journal of Shanghai Jiaotong University (in Chinese), to be published, DOI: 10.16183/j.cnki.jsjtu.2023.545.
- [8] Wang K., Sun H., Zhang L. et al., An overview of rotor pole optimization techniques for permanent magnet synchronous machines, Proceedings of the CSEE (in Chinese), vol. 37, no. 24, pp. 7304–7317 (2017), DOI: 10.13334/j.0258-8013.pcsee.170673.
- [9] Xu Yuanyuan, Ge Hongjuan, Jing Yan, *Optimal design of eccentric magnet pole for permanent-magnet synchronous motors*, Journal of Harbin Engineering University (in Chinese), vol. 34, no. 7, pp. 873–877 (2013), DOI: 10.3969/j.issn.1006-7043.201210016.

- [10] Qi Xin, Wu Xinzhen, Optimization method of eccentricity cutting technology for surface-mounted permanent magnet motor, Large Electric Machine and Hydraulic Turbine (in Chinese), vol. 2019, no. 6, pp. 25–29 (2019), available online on: https://kns.cnki.net/kcms2/article/abstract?v=bTgd32KJj6sibcfWKyUyR_9sAMI50V9oLqdHWiKQD_WUNSkUxUYSt660WTh1GlkpJUVe2HxR 2EoFuY-1y_0IlcitCZoJ-XJa-qiEjajzM5W9Dui6BLEA0Wot7_MsPOI0kaKYtIZq9Cdl0s840eEEpkDfb 8ekOGkIffXHDz1pe40Ak_SPLibfGV1gWO9MvtafkxX4940HGZA=
- [11] Verma M., Singh M., Sreejeth M., Integrated Taguchi method-assisted polynomial metamodelling & genetic algorithm based optimisation of a surface inset permanent synchronous motor for performance improvement, IET Electrical Systems in Transportation, vol. 12, no. 1, pp. 26–35 (2022), DOI: 10.1049/els2.12035.
- [12] Gao Fengyang, Gao Jianning, Li Mingming, Yao Pu, Song Zhixiang, Yang Kaiwen, Gao Huanyu, *Optimization design of Halbach interior permanent magnet synchronous motor based on parameter sensitivity stratification*, Journal of Xi'an Jiaotong University (in Chinese), vol. 56, no. 5, pp. 180–190 (2022), DOI: 10.7652/xjtuxb202205018.
- [13] Qiao Zizhuo, Zhang Pengjun, Yu Yunfeng, Shi Zhiyu, Liu Qi, Guo Wei, Bai Yun, Zhang Yun, *Optimization design of improved Halbach permanent magnet synchronous*, Journal of Gun Launch & Control (in Chinese), to be published, DOI: 10.19323/j.issn.1673-6524.202409009.
- [14] Hua Yizhou, Liu Yichen, Pan Wei, Diao Xiaoyan, Zhu Huangqiu, Multi-objective optimization design of bearingless permanent magnet synchronous motor using improved particle swarm optimization algorithm, Proceedings of the CSEE, vol. 43, no. 11, pp. 4443–4452 (2023), DOI: 10.13334/j.0258-8013.pcsee.220039.
- [15] Qiao Lukuan, Zhang Bingyi, Li Yan, Feng Jiahong, Multi-objective optimization design of external rotor permanent magnet synchronous motor based on improved particle swarm optimization algorithm, Electric Machines & Control Application (in Chinese), vol. 50, no. 3, pp. 81–87+94 (2023), DOI: 10.12177/emca.2022.176.
- [16] Huang Chaozhi, Zhang Wenjin, Li Haiwen, Sun Yanwen, *Application of multi-objective algorithm layered optimization strategy in switched reluctance motor*, Journal of Electronic Measurement and Instrumentation (in Chinese), vol. 38, no. 1, pp. 124–133 (2024), DOI: 10.13382/j.jemi.B2306822.
- [17] Liu Xiping, Fu Jiesheng, Du Longxin, Guo Gaosheng, Zhu Wenjian, *Analysis and optimization design of IPMSM with a double-layer permanent magnet structure of electric vehicles*, Automotive Engineering (in Chinese), vol. 43, no. 8, pp. 1128–1135 (2021), DOI: 10.19562/j.chinasae.qcgc.2021.08.002.
- [18] Qiu Mashun, Hua Qingsong, *Electromagnetically optimized design for high-speed permanent magnet synchronous motor by Taguchi iteration*, Journal of Beijing Normal University (Natural Science) (in Chinese), vol. 58, no. 5, pp. 713–719 (2022), DOI: 10.12202/j.0476-0301.2022122.
- [19] Zhang Yufeng, Gao Wentao, Shi Qiaoning, Meng Qingpin, Du Guanghui, *Optimization design of dual-redundancy permanent magnet synchronous motor based on improved iterations Taguchi method*, Transactions of China Electrotechnical Society (in Chinese), vol. 38, no. 10, pp. 2637–2647+2685 (2023), DOI: 10.19595/j.cnki.1000-6753.tces.220768.
- [20] Li Xiaohua, Li Guangxu, Han Zhongchuan, Han Xu, Wei Shurong, High-torque and low-noise IPMSM multi-objective collaborative optimization based on multi-layer surrogate model, Advanced Technology of Electrical Engineering and Energy (in Chinese), vol. 44, no. 2, pp. 1–12 (2025), DOI: 10.12067/ATEEE2403004.
- [21] Shami T.M., Mirjalili S., Al-Eryani Y., Daoudi K., Izadi S., Abualigah L., *Velocity pausing particle swarm optimization: A novel variant for global optimization*, Neural Computing and Applications, vol. 35, no. 12, pp. 9193–9223 (2023), DOI: 10.1007/s00521-022-08179-0.